Journal of Engineering and Applied Research (JEAR)

National University of Skills

Summer & Autumn 2025, Vol. 2, No. 2, p. 226- 244

Journal Homepage: https://jear.tvu.ac.ir

:10.48301/JEAR.2024.474745.1075

ANFIS-Based Speed Control of Switched Reluctance Generators for Wind Energy Systems

Reza Ghanizadeh[1*], Amir Parsafar[2]

[1]Department of Electrical Engineering, Ur.C., Islamic Azad University, Urmia, Iran.
[2]Department of Electrical Engineering, Artificial Intelligence and Big Data Automation Research Center, Ur.C., Islamic Azad University, Urmia, Iran.

ARTICLE INFO

Article Type:
Original Research

Received: 01.22.2025
Revised: 06.04.2025
Accepted: 04.11.2025

Keyword:
Switched Reluctance Generator
Variable Speed Generator
Adaptive Control
Wind Turbine
Neuro-Fuzzy Inference System

***Corresponding Author:**
Reza Ghanizadeh
Email:
reza.ghanizadeh@iau.ac.ir

ABSTRACT

Due to their variable speed operation, the use of switched reluctance generators (SRGs) in wind energy systems is more complex compared to conventional generators in this industry. The unique structure of SRGs makes their control more challenging. However, their simple and robust construction, along with lower cost, makes them an attractive option for wind turbines. This paper introduces a novel approach for controlling the speed of SRGs using an Adaptive Neuro-Fuzzy Inference System (ANFIS) controller. In this setup, the SRG is powered by a variable speed wind turbine and connected to the power grid through an asymmetric half-bridge converter, a DC-link, and a DC-AC inverter. Effective speed regulation is essential to maximize power output at varying wind speeds. We provide a comprehensive analysis of the SRG's modeling and control strategies, along with detailed descriptions of the wind turbine, converter, and inverter components. The proposed system's performance is validated through simulations based on variable wind speed data with Matlab/Simulink demonstrate the efficacy and robustness of our control methodology.

©2024 the authors. Published by National University of Skills, Tehran, Iran. This article is an open-access article distributed under the terms and conditions of the Creative Commons Attribution-Noncommercial 4.0 International (CC BY-NC 4.0 license) (https://creativecommons.org/licenses/by-nc/4.0/).

E-ISSN: 3060-6357

Introduction

Wind energy is rapidly emerging as a major global power source. In 2023, the wind industry globally set a new record by adding 117 gigawatts (GW) of new capacity, marking a 50% rise compared to the previous year. This swift growth is driven by the desire of many nations to enhance their energy security. Moreover, the environmental advantages of wind energy, such as the reduction of greenhouse gas emissions and decreased dependence on fossil fuels, play a crucial role. The scalability and decreasing costs of wind energy technology also significantly contribute to its accelerated adoption and expansion [1].

Fixed-speed wind energy conversion systems (WECS) are simple electrical machines that consist of an aerodynamic rotor linked to a gearbox and shaft, which in turn drive a squirrel cage induction generator (SCIG) [2-4] or a wound rotor induction generator (WRIG) [5; 6]. Operating at a constant speed regardless of wind conditions can reduce aerodynamic efficiency and may cause rotor blade noise issues at low wind speeds. The energy efficiency of variable-speed wind turbines is significantly higher compared to fixed-speed turbines. Consequently, these systems are now more commonly used [7].

Switched Reluctance Generators offer distinct benefits due to their unique operational principles. By eliminating the need for magnets and employing a passive rotor, the SRG simplifies its design and reduces manufacturing costs [8]. The rotor's design minimizes heat dissipation and can even facilitate cooling of the stator, thereby enhancing the machine’s tolerance to elevated temperatures [9]. This efficient cooling process also makes it easier to achieve a hermetic construction. Additionally, the passive rotor contributes to reduced copper winding losses, as it is devoid of any conductive components [10]. The SRG exhibits superior power-to-weight and torque-to-weight ratios compared to traditional electrical machines. Its phase-independent structure enhances its robustness, making it highly resistant to faults such as open-coil issues and power converter malfunctions [11]. In various applications, SRGs demonstrate exceptional reliability and efficiency. For low-speed operations, including wind turbines [12-14] and water turbines [15], the lack of magnets not only lowers production costs but also eliminates cogging torque. In high-speed scenarios, such as in steam and gas turbines or micro-CHP systems, the SRG’s design allows for the omission of gearboxes, streamlining electric power systems [16].

SRGs possess unique operational benefits, making them an excellent option for wind energy applications. An extensive review covers their foundational principles, control methodologies, and future research avenues, showcasing SRGs' flexibility and efficiency for modern wind energy systems [17]. Different excitation methods, including separate field current and circulating current excitations, have been analyzed for SRGs [18]. To enhance power quality, adaptive filter-based techniques have been investigated [19]. Ensuring stable SRG operation when supplying constant power

loads in DC microgrids has been crucial for their reliable integration into contemporary grid systems [20]. Additionally, SRG integration into microgrids with plug-in energy support mechanisms has demonstrated improved reliability and efficiency in decentralized energy systems [21]. Efficiency optimization remains a key focus, with strategies utilizing position sensor-less control techniques aimed at reducing system complexity and enhancing overall efficiency [22]. For small-scale wind power setups, effective control strategies for power converters are essential to ensure efficient power conversion and stable operation, even in low wind conditions [23]. Finally, defining control objectives to boost SRG performance in generating mode contributes significantly to their reliable and efficient conversion of wind energy into electrical power [24].

This paper introduces a novel approach to speed control for the switched reluctance generator (SRG) utilizing an adaptive neuro-fuzzy inference system controller. The SRG, driven by a variable-speed wind turbine, is connected to the grid via an asymmetric half-bridge converter, DC-link, and DC-AC inverter system. Effective speed control is crucial for the variable-speed operation of the SRG to ensure optimal power delivery to the grid at varying wind speeds. This study provides comprehensive modeling and control strategies for the SRG and its associated components, including the wind turbine, converter, and inverter systems. The proposed system's performance is validated through simulation results, using variable wind speed data. The dynamic simulations are conducted using Matlab/Simulink.

Proposed system

Mathematical Model of Wind Turbine

The power P generated by the wind, derived from the kinetic energy's rate of change, can be expressed as:

$$P = \frac{1}{2}\rho A v_{\omega}^{3} \tag{1}$$

where ρ and A denote the air density and the effective are, respectively and v_{ω} indicates velocity of wind. The mechanical power P_{ω} harnessed by the rotor blades is determined by the difference between the wind power before (v_i) and after the rotor blades (v_o), which is:

$$P_{\omega} = \frac{1}{2}\rho A v_{\omega}(v_i^2 - v_o^2) \tag{2}$$

Utilizing the mass flow rate, we can formulate the following:

$$\rho A v_{\omega\alpha} = \frac{\rho A(v_i + v_o)}{2} \tag{3}$$

where $v_{\omega\alpha}$ is the average velocity of wind. We can rewrite (2) as follows [25].

$$P_{\omega} = \frac{1}{2}\rho A \frac{(v_i + v_o)}{2}(v_i^2 - v_o^2) = \frac{1}{2}\rho A v_i^3 C_p \tag{4}$$

$$C_p = \frac{1}{2}\left[1 - (\frac{v_i}{v_o})^2 + (\frac{v_i}{v_o}) - (\frac{v_i}{v_o})^3\right] \tag{5}$$

The power coefficient C_p, representing the rotor's efficiency, depends on the tip speed ratio τ and the blade pitch angle α [degrees] and may be written as follows [26].

$$C_p = \frac{1}{2}\left[\gamma - 0.02\alpha^2 - 5.6\right]e^{-0.17\gamma} \tag{6}$$

$$\tau = \frac{\omega_{mR}}{v_{\omega}}, \quad \gamma = \frac{R}{\tau}, \frac{3600}{1609} \tag{7}$$

where ω_m denotes the rotational speed in rad/s and R is the turbine blade radius.

Maximum Power Generation

In variable speed wind turbine generator systems, the active power produced is influenced by the power coefficient, C_p, which signifies the fraction of power harnessed from the wind. The ideal values for the tip speed ratio and power coefficient are determined based on the turbine's characteristics. For every given wind speed of a variable speed wind turbine, there exists a specific rotational speed that yields the maximum active power $P_{\omega max}$ from the wind generator. This study presents the power coefficient curve with the maximum power point tracking (MPPT) line in Figure 1. Due to the challenge of accurately measuring wind speed, it is more effective to compute the maximum power $P_{\omega max}$ without directly measuring wind speed, using the following formula:

$$P_{\omega \max} = \frac{1}{2}\rho A \frac{\omega_r R}{\tau_{opt}} C_{p-opt} \tag{8}$$

where τ_{opt} denotes the optimum tip speed ratio and may be expressed based on the turbine mathematical equations. Equation (8) demonstrates that the maximum power output is directly proportional to the cube of the rotational speed. The pitch converter operates to regulate the mechanical torque of the wind turbine when the rotor speed surpasses the rated speed.

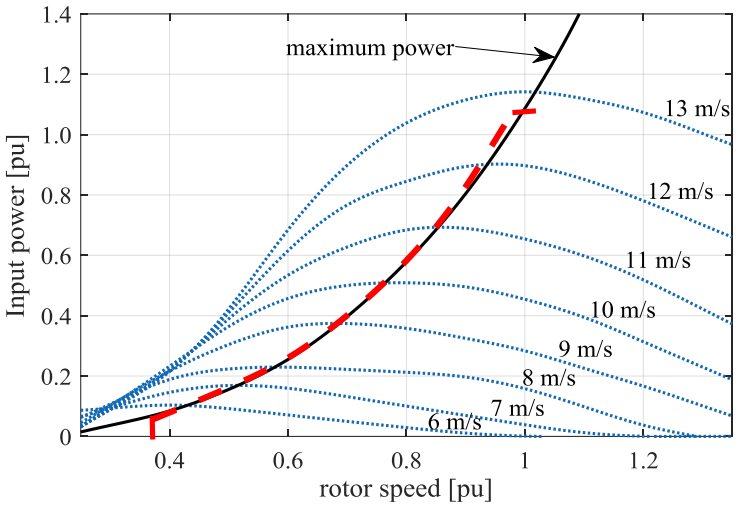

Figure 1. Maximum power point line for wind turbine at different speeds.

Dynamic Equations of the SRG

A wind turbine transforms the kinetic energy of wind into mechanical energy, which is then transferred to the SRG to produce electrical energy. Based on equation (4), the mechanical torque T_ω exerted on the wind turbine shaft is defined as follows.

$$T_\omega = \frac{1}{2}\rho AR\frac{C_p}{\lambda}v_\omega^2 \tag{9}$$

The dynamic equation for the SRG is expressed as follows:

$$J\frac{d\omega_m}{dt} = T_\omega - T_e \tag{10}$$

In this context, J represents the moment of inertia, and T_e denotes the total torque generated by the phases of the generator. Figure 2(a) and Figure 2(b) display the proposed four-phase 8/6 SRG and the used four-phase half-bridge converter (AHBC), respectively. The specifications of the desired generator are also given in Table 1.

In a switched reluctance machine, the phase inductance reaches its peak when the stator and rotor poles are fully aligned, resulting in the lowest reluctance. As the rotor pole moves away from this aligned position, the current in the stator windings decreases, causing the inductance to drop to its minimum value. Torque production in an SRG is influenced by the magnetic field, which aims to align the poles to achieve minimal reluctance. The SRG generates torque by synchronizing excitation with the rotor's position [27]. When the poles start to separate, the reluctance increases, leading to the creation of negative torque. Under linear operating

conditions, the torque generated by a phase in an SRG can be calculated as shown (11).

$$T_e = \frac{1}{2} t^2 \frac{dL}{d\theta} \tag{11}$$

In this context, T_e represents the electromagnetic torque, i stands for phase current, L is the phase inductance, and θ indicates the rotor position. Since the SRG operates in a region where the inductance decreases (d_L/d_θ=0), the torque generated is negative. The total torque produced by the four-phase generator in this study is the aggregate of the torques from each individual phase.

Table 1. Specifications of the SRG

Generator technical specifications	Value
DC voltage	220 V
Maximum phase current	180 A
Nominal torque	160 N m
Nominal speed	3500 rpm
Number of phases	4
Number of poles	8/6
Winding resistance	0.05 Ω
Moment inertia	0.06 kg m2
Friction coefficient	0.02 Nms

In the SRG, each phase winding must be energized in a specific sequence. To achieve this, an electronic driver circuit is essential for directing current through the phases based on the rotor's position. Various driver circuits for controlling Switched Reluctance Machines are discussed in the literature. For this study, we utilized the asymmetric half-bridge converter (AHBC) depicted in Figure 2(b) to operate the SRG. This driver circuit consists of two diodes and two switches per phase. Phase voltage in a switched reluctance machine may be written as:

$$V_k = r.\mathrm{i_k} + \frac{d\varphi_k}{dt} \tag{12}$$

where, r and i_k indicate the phase winding resistance and phase current, respectively, while ψ_k denotes phase magnetic flux that can be written as:

$$\varphi_k = L_\mathrm{k}(i,\theta).i_k \tag{13}$$

Finally, considering $\omega=d_L/d_\theta$, the phase voltage can be expressed as follows:

$$V_k = r.i_\mathrm{k} + L_k \frac{di}{dt} + e_k \tag{14}$$

$$e_k = i_\mathrm{k}.\omega \frac{dL_k}{d\theta} \tag{15}$$

where, e_k denotes the back electromotive force.

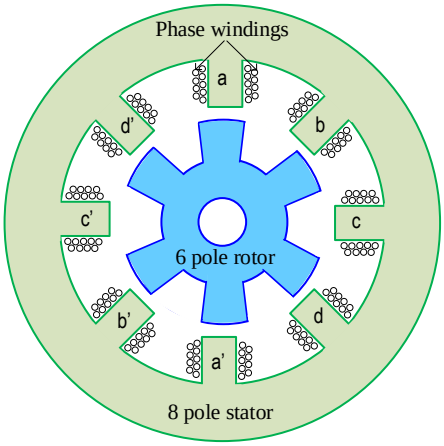

(a)

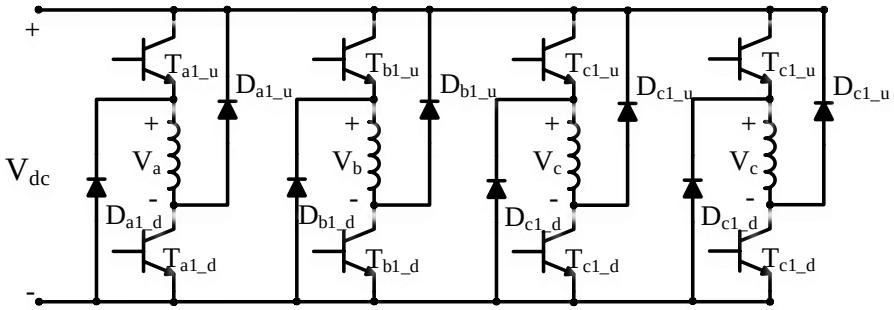

(b)

Figure 2. (a) proposed SRG, (b) AHBC

Magnetization characteristics of the proposed SRG is shown in Figure 3. To achieve generating mode operation, the applied voltage remains positive throughout the conduction period, defined as the interval between the switch-on (θ_{no}) and switch-off (θ_{off}) angles. After the switch-off angle, the voltage turns negative until the extinction angle (θ_{ex}), where the phase current drops to zero. At all other times, the voltage is zero. The magnetic flux linkage curve, along with the phase current and reluctance torque for the specific switched reluctance machine, is illustrated in Figure 4. These curves are derived considering firing and switching-off angles of 10 degrees and 30 degrees, respectively, under nominal load and a speed of 2000 rpm.

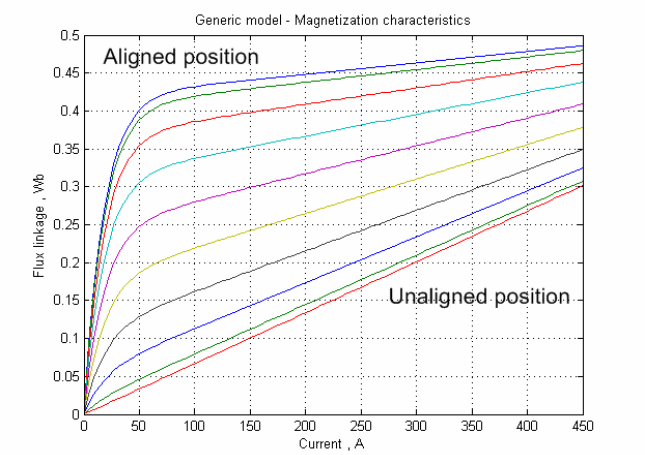

Figure 3. Magnetization characteristics of the proposed SRG

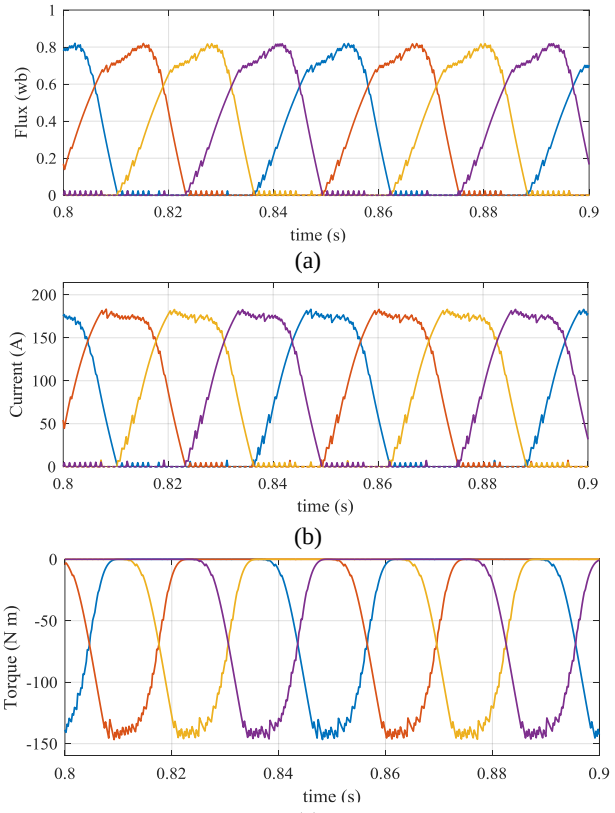

Figure 4. SRG performance under nominal load and constant on and off angles, (a) flux linkage, (b) phase current, (c) phase torque.

Control system

The suggested control system is divided into two parts: speed regulation managed by the AHBC, and DC link voltage control achieved through the grid-side converter, as depicted in Figure 5.

Dynamic Equations of the SRG

The aim of this control unit is to regulate the speed of the SRG. The generator operates by delaying the fire angles so that the conduction period occurs after the aligned position, where phase inductance decreases and d_L/d_θ is negative. In this scenario, the energy returned to the DC-link during the de-fluxing period (P_θ) exceeds the excitation energy supplied during the dwell period (P_{ex}), with the difference provided by the prime mover. The electrical output power is given by (16).

$$P_{out} = P_o - P_{ex} \tag{16}$$

During the conduction period, the applied voltage is positive, which spans from the switching on angle (θ_{no}) to the switching off angle (θ_{off}). After the switching off angle until the extinction angle (θ_{ex}), which corresponds to zero phase current, the voltage becomes negative. In all other instances, the voltage is zero. For optimal performance, the switching on angle must be set after the aligned position ($0°$) to ensure the conduction period follows this position, where d_L/d_θ is negative. The reference signal for this operation is determined using the maximum power point tracking (MPPT) algorithm described in section 2. The conduction signals are generated based on this logic, and a hysteresis controller effectively generates the optimal firing angles for the inverter to maximize the generator's output power according to the reference signal. The optimum rotor speed is maintained using an adaptive neuro-fuzzy inference system controller, which manages the switching on angle (θ_{on}) as detailed in section 4.

DC Link Voltage Control

As illustrated in Figure 5, the primary goal of the grid-side inverter is to maintain the DC link voltage, enabling the active power produced by the SRG to be effectively delivered to the grid. In this figure, the subscript g represents parameters related to the grid. The inverter utilized is space vector PWM-based voltage source system presented in [28]. The control strategy employs *d-q* reference frames, where the *d*-axis is aligned with the system voltage. The transformation angle is derived from the three-phase voltages (V_{abc}) at the high-voltage side of the grid-side transformer. This configuration allows the direct current component I_d of the inverter to manage active power, while the quadrature current component I_q regulates reactive power. The specified DC-link voltage is 220 V. The *PI* controller gains were determined using a trial-and-error method and these gains are listed in Table 2.

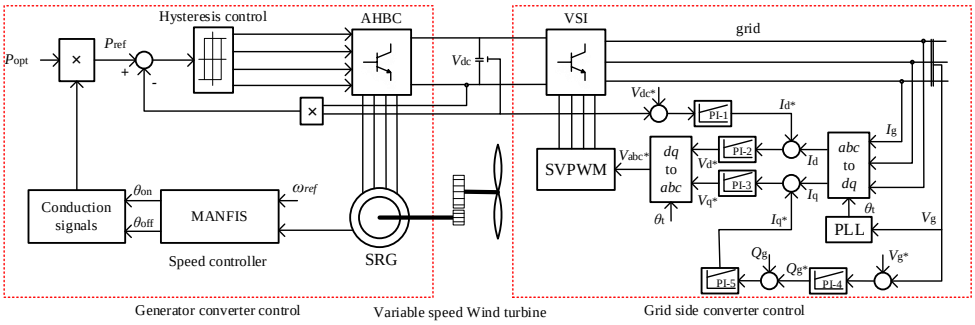

Figure 5. Block diagram of the system

Table 2. Gains of PI controllers in grid side

PI	Integral gain	Proportional gain
1	0.72	13.5
2	2.32	4.61
3	1.85	4.61
4	15.91	8.85
5	9.65	27.33

Adaptive neuro fuzzy inference system

Adaptive Neuro-Fuzzy Inference System (ANFIS) is a hybrid model combining fuzzy logic and neural networks. This model is highly effective in managing nonlinear systems without needing exhaustive data about the complex system. The Takagi-Sugeno inference system defines the inputs for the system, while the neural network enhances the fuzzy system by providing learning capabilities and parameter adjustments.

ANFIS delivers accurate results without the necessity for separate input or output network computations. The structure of ANFIS comprises five layers, as illustrated in Figure 6.

Layer 1: Each node in this layer represents a node function. This layer maps the degree of membership of the input parameters to the corresponding fuzzy sets. In this context, a generalized bell membership function is utilized, and the degree is calculated as per (17). Here, c_k and b_k are the center and half-width of the membership function, respectively, while b adjusts the slopes at the crossover points. x is the input to the k^{th} node, and A_k represents the linguistic label.

$$\mu_{Ax}(x) = gbell(x; a_k, b_k, c_k) = 1/(1+\left|\frac{x_k - c_k}{a_k}\right|), k = 1,2 \quad (17)$$

Layer 2: Nodes compute their activation levels using the following equation:

$$W_k = \mu_{Ak}(x) \times \mu_{Ak}(z), k = 1,2 \tag{18}$$

where z represents the input to the k^{th} node and B_k is the associated linguistic label.

Layer 3: Activation levels from layer 2 are normalized for all rules according to (19), where W_k denotes the activation level determined by (18).

$$\bar{W}_k = W_i / (W_1 + W_2), k = 1,2 \tag{19}$$

Layer 4: This layer processes the normalized parameters and sets. The contribution of the k^{th} rule to the overall output, denoted as f_k, is calculated by node k as (20), where $\{p_k, q_k, d_k\}$ represents the parameter set and $\bar{w}_k$ is the normalized activation level from layer 3.

$$\bar{W}_k \times f_k = \bar{W}_k (p_k \times x + q_k \times z + d_k), k = 1,2 \tag{20}$$

Layer 5: This layer performs the defuzzification process by computing the outputs as the aggregate contribution from each rule:

$$\sum_k \bar{W}_k \times f_k = \frac{\sum_k W_k \times f_k}{\sum_k W_k}, k = 1,2 \tag{21}$$

To optimize the parameters of the ANFIS model, a systematic approach was adopted. The training dataset used for the ANFIS model consists of speed error and its rate of change as the inputs, with the goal of minimizing the speed error in the SRG system. The selection of membership functions for the ANFIS system involved using a generalized bell-shaped membership function, which provides good flexibility for the modeling of nonlinear systems.

The parameters of the ANFIS model, such as the center and half-width of the membership functions, were optimized using the gradient descent method during the training phase. The error signal generated by the ANFIS was used to adjust the local parameters in the model, with updates being performed iteratively. The optimization process ensures that the model adapts to varying system conditions, thereby improving the accuracy and performance of the speed control. As part of the training procedure, the system undergoes backpropagation, where the local parameters are updated according to the error signal. The optimization of these parameters is critical to achieving the desired performance in terms of speed regulation and overall control accuracy.

The Multi Output Adaptive Neuro-Fuzzy Inference System (MANFIS) is an extension of ANFIS designed to produce multiple outputs. As depicted in Fig. 6, ANFIS typically generates a single output, whereas MANFIS can combine several independent ANFIS units to produce multiple outputs [29].

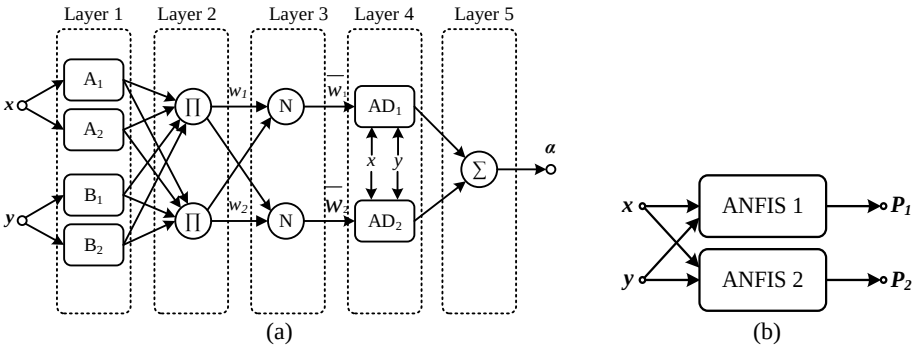

Figure 6. (a) adaptive neuro fuzzy system (ANFIS), (b) Multi output ANFIS

In this study, the speed control of the SRG is achieved using a MANFIS. The speed error and its rate of change serve as inputs for the respective phase MANFIS. The developed controller generates firing pulses for the converter switches to reduce the error. Figure 6 illustrates the system, where circles denote fixed nodes and squares represent adaptive nodes. The rule base consists of two Takagi-Sugeno type if-then rules:

Rule 1: If x is A_1 and z is B_1, then $f_1=p_1x+q_1z+d_1$,

Rule 2: If x is A_2 and z is B_2, then $f_2=p_2x+q_2z+d_2$,

In these rules, A_k and B_k are fuzzy sets, and (p_k,q_k,d_k) are parameters of the output function. For the j-th rule, the firing interval is given by:

$$W_j(\gamma(t)) \in \left[\underline{\omega}_j(\gamma(t)), \bar{\omega}_j(\gamma(t))\right] \tag{22}$$

with $\underline{\omega}_j(\gamma(t))$ and $\bar{\omega}_j(\gamma(t))$ defined as follows:

$$\underline{\omega}_j(\gamma(t)) = \varphi_{M_1^j}(f_1(\gamma(t)) \times ... \times \underline{\varphi}_{M_\mu^j}(f_\mu(\gamma(t)) \tag{23}$$

$$\bar{\omega}_j(\gamma(t)) = \bar{\varphi}_{M_1^j}(f_1(\gamma(t)) \times ... \times \bar{\varphi}_{M_\mu^j}(f_\mu(\gamma(t)) \geq 0 \tag{24}$$

Here, $\varphi_{M_1^j}$ and $\bar{\varphi}_{M_1^j}$ are the lower and upper membership functions, ranging between [0, 1]. For all j and t $\geq$ 0, $\bar{\omega}_j(\gamma(t))$ is always greater than or equal to $\underline{\omega}_j(\gamma(t))$. The defuzzification of the k-th local system, with membership grade $\omega_j(\gamma(t))$, is expressed as:

$$\dot{x}_j(t) = \sum_{j=1}^{p} \omega_j(\gamma(t))(A_j x(t) + B_j u(t)) \tag{25}$$

To accommodate uncertain parameter variations, two weighting coefficient functions, $\underline{\delta}_k(\gamma(t))$ and $\bar{\delta}_k(\gamma(t))$, are incorporated into the j-th subsystem membership function:

$$\omega_j(\gamma(t)) = \underline{\delta}_k(\gamma(t))\underline{\omega}_j(\gamma(t)) + \bar{\delta}_k(\gamma(t))\bar{\omega}_j(\gamma(t)) \geq 0 \tag{26}$$

$$0 \le \underline{\delta}_k(\gamma(t)) \le 1, \qquad 0 \le \overline{\delta}_k(\gamma(t)) \le 1 \tag{27}$$

$$\sum_{j=1}^{p} \omega_j(\gamma(t)) = 1, \qquad \underline{\delta}_k(\gamma(t)) + \overline{\delta}_k(\gamma(t)) = 1 \tag{28}$$

An adaptive sliding mode controller is devised and applied to the IT fuzzy model of the SRG. It is assumed that the weight $\overline{\delta}_k(\gamma(t))$ of the *j*-th membership grade function has an upper limit (ξ_j):

$$0 \le \overline{\delta}_k(\gamma(t)) \le \xi_j \le 1 \tag{29}$$

Thus,

$$0 \le 1 - \xi_j \le \underline{\delta}_k(\gamma(t)) \le 1 \tag{30}$$

During the back-propagation phase, the error signal is propagated backwards, updating local parameters via the gradient descent method. For a neuro-fuzzy system with a single output, α, this process is represented by (31):

$$\delta_{ki}(t+1) = \delta_{ki}(t) - (\tau / \rho).(\partial CF / \partial \delta_{ki}) \tag{31}$$

where, τ is the training rate of μ_k, ρ is the count of input or output data, and CF is the quadratic cost function. Partial derivatives, calculated as per the rule in (32), are used to update the membership function parameters:

$$\frac{\partial CF}{\partial \delta_k} = \frac{\partial CF}{\partial \alpha} \cdot \frac{\partial \alpha}{\partial \alpha_k} \cdot \frac{\partial \alpha_k}{\partial w_k} \cdot \frac{\partial w_k}{\partial \mu} \cdot \frac{\partial \mu}{\partial \delta_k} \tag{32}$$

For local parameter adjustment, the MANFIS model with two outputs sums the gradients from both output errors (e_1 and e_2):

$$\delta_{ki}(t+1) = \delta_{ki}(t+1) - (\tau / \rho).\left(\frac{\partial CF_1}{\partial \delta_{ki}} + \frac{\partial CF_2}{\partial \delta_{ki}}\right) \tag{33}$$

where $\frac{\partial CF_1}{\partial \delta_{ki}} = f(e_1)$ and $\frac{\partial CF_2}{\partial \delta_{ki}} = f(e_2)$.

The described MANFIS is utilized to control phase force and generate converter pulses. Each motor phase has its own MANFIS. The fuzzification unit has two inputs: force error and change in error. Table 3 lists the rules for the fuzzy unit, including NB (negative big), *NM* (negative medium), *NS* (negative small), *Z* (zero), *PS* (positive small), *PM* (positive medium), and PB (positive big). The neural network determines the appropriate rule, generating a control signal to achieve optimal output. The final defuzzification unit provides firing pulses for the converter.

Table 3. Rules of fuzzy inference system

		Δe						
		NB	*NM*	*NS*	*Z*	*PS*	*PM*	*PB*
e	*NB*	*NB*	*NB*	*NB*	*NM*	*NM*	*NS*	*Z*
	NM	*NB*	*NB*	*NM*	*NS*	*NS*	*Z*	*PS*

NS	*NB*	*NM*	*NS*	*NS*	*Z*	*PS*	*PM*
Z	*NM*	*NS*	*NS*	*Z*	*PS*	*PS*	*PM*
PS	*NM*	*NS*	*Z*	*PS*	*PS*	*PM*	*PB*
PM	*NS*	*Z*	*PS*	*PS*	*PM*	*PB*	*PB*
PB	*Z*	*PS*	*PM*	*PM*	*PB*	*PB*	*PB*

Simulation results

The designed system comprises a Switched Reluctance Generator (SRG) connected to an asymmetric half-bridge converter, a DC-link capacitor, a grid-side inverter, and the power grid. Simulations were performed in Matlab/Simulink to analyze the system's performance under varying wind conditions, focusing on dynamic response, power regulation, and control robustness.

Figure 7 illustrates the wind speed profile used during the simulations, representing rapid fluctuations and gradual variations to evaluate the adaptability of the proposed control system. These variations emulate real-world wind patterns to ensure that the system performs effectively in practical scenarios.

The primary objective of the control strategy is to maximize wind energy capture by dynamically adjusting the SRG rotor speed according to real-time wind speed, while ensuring that the generated power remains within the rated capacity of the generator. To achieve this, a chopped current control mode is employed for the SRG, which limits the current and protects the asymmetric half-bridge inverter from overcurrent conditions.

Figure 8 shows a comparison between the actual rotor speed of the SRG and the optimal rotor speed calculated using the Maximum Power Point Tracking (MPPT) algorithm. The close alignment between the two curves throughout the wind variations indicates the effectiveness of the proposed MANFIS-based controller in maintaining near-optimal operating conditions. This ensures that the system extracts the maximum possible power from the wind at each moment.

Figure 9 presents the active and reactive power outputs at the grid-side converter. As seen in subfigure (a), the active power follows the variations in wind speed and generation, while subfigure (b) shows how the reactive power is regulated to maintain power factor and grid stability. The power measurements are based on the voltage and current provided to the DC-link capacitor, captured through accurate transducers.

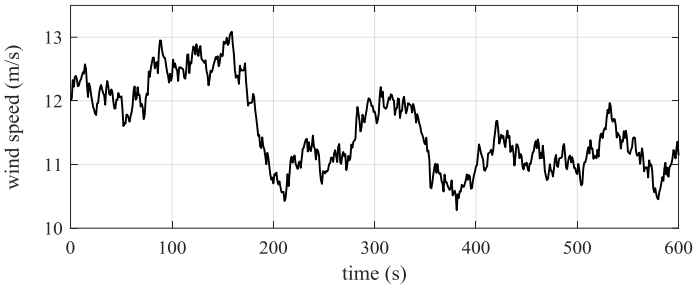

Figure 7. Wind speed profile used in evaluations

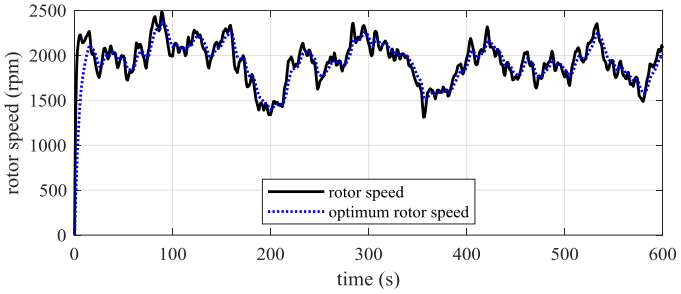

Figure 8. Rotor speed of the SRG at variable wind speed

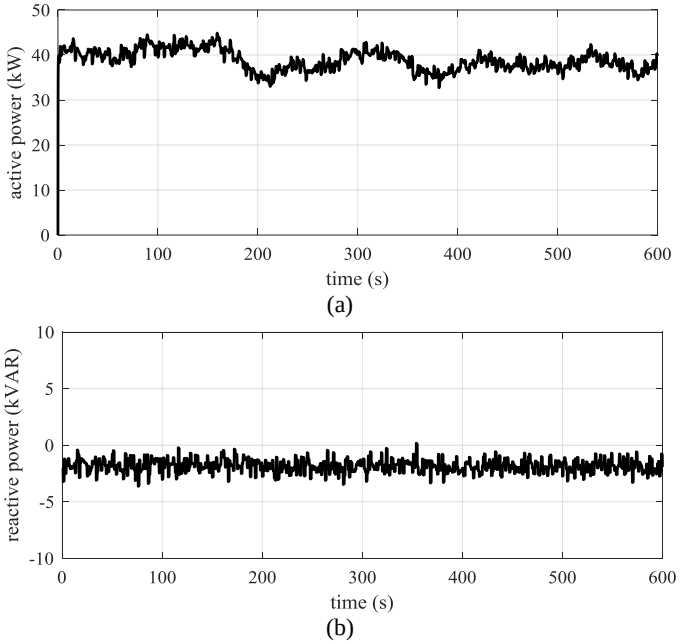

Figure 9. Power at the gride side converter, (a) active power, (b) reactive power,

Figure 10 depicts the DC-link voltage at the output of the SRG. The voltage is regulated around 220 V with a narrow regulation bandwidth of 5 Hz, indicating a

fast and stable response by the front-end converter. This regulation is achieved by dynamically adjusting the direct current component injected into the grid, enabling efficient power delivery and system stability. The simulation results confirm the reliable performance of the front-end control loop and its ability to maintain voltage stability under different loading and generation conditions.

In summary, the proposed control scheme demonstrates strong dynamic performance, effective voltage regulation, and efficient wind energy capture, validating the functionality of the system under realistic and challenging operating conditions.

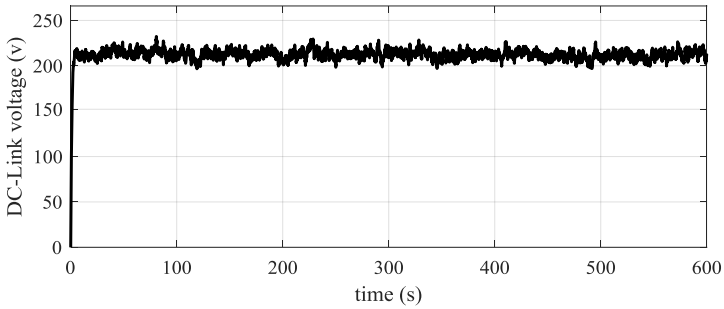

Figure 10. DC-Link voltage

To provide a better assessment of the system's performance, a comparison with the results presented in [30] has been conducted. The key differences are summarized in Table 4.

Table 4. results comparison

	MPPT	Method in [30]
Tracking accuracy	1 %	1.5 %
Dc-link voltage fluctuations	± 8 v	± 11 v
Dynamic time in response in second	1 s	1 s

Conclusion

This paper proposed an ANFIS-based control algorithm for regulating the speed of Switched Reluctance Generators (SRGs) in wind energy systems. The inherent complexity and variable speed operation of SRGs introduce substantial control challenges, but their robust, cost-effective nature makes them ideal for wind turbine applications. The proposed system integrates a variable-speed wind turbine, an asymmetric half-bridge converter, a DC-link capacitor, and a DC-AC inverter to optimize power output under varying wind conditions. The ANFIS controller was shown to significantly enhance the system's performance, as confirmed through Matlab/Simulink simulations. The results highlighted key advantages such as improved speed regulation, higher efficiency, and greater system stability, all of

which demonstrate the effectiveness of the proposed approach. These improvements are critical for advancing SRG technology in renewable energy applications. Future work will focus on refining the control algorithms further and exploring real-world testing to validate these promising results.

Disclosure statement and funding

The authors declare no potential conflicts of interest. The present study received no financial support from any organization or institution.

References

[1] Mishra, S., & Manhas, N. S. (2023). Promoting Green Energy Transition Through G20. *India Quarterly*, *79*(4), 552-563. https://doi.org/10.1177/097492842312033 45.

[2] Satpathy, A. S., Kastha, D., & Kishore, N. K. (2021). Vienna rectifier-fed squirrel cage induction generator based stand-alone wind energy conversion system. *IEEE Transactions on Power Electronics*, *36*(9), 10186-10198. https://doi.org/10 .1109/TPEL.2021.3062694

[3] Abi Narwastu, M., & Riyadi, S. (2022, December 13-14). *Analysis of Squirrel Cage Induction Machine in Motoring and Generating Operation*. 6th International Conference on Information Technology, Information Systems and Electrical Engineering (ICITISEE), Yogyakarta, Indonesia. https://doi.org/10.1109/ICIT ISEE57756.2022.10057928

[4] Huang, R., Li, H., Fei, F., Qi, Y., Song, T., & Zheng, S. (2023, November24-26). *Research on a New Control Method of Squirrel Cage Induction Generator for Wind Turbine*. 3rd International Conference on New Energy and Power Engineering (ICNEPE), Huzhou, China. https://doi.org/10.1109/ICNEPE60694.2023.104 29442

[5] Meena, P., Prema, V., Bhaskar, M. S., & Almakhles, D. (2021). Bi-Furcated Stator Winding Configuration in Three-Phase Induction Generators for Wind Power Generation. *IEEE Access*, *9*, 153188-153198. https://doi.org/10.1109/ACCESS .2021.3127526

[6] Ketabipour, S., Samet, H., Mohammadi, M., Li, Q., & Terzija, V. (2023). Modeling of Extremely Short-Time Power Variations of Wound Rotor Induction Machines Wind Farms for Flicker Studies. *IEEE Access*, *11*, 135556-135567. https://doi.org/10.1109/ACCESS.2023.3337388

[7] Mansour, M., Mansouri, M. N., & Mimouni, M. F. (2011, March 3-5). *Comparative study of fixed speed and variable speed wind generator with pitch angle control.* IEEE International Conference on Communications, Computing and Control Applications (CCCA), Hammamet, Tunisia https://doi.org/10.1109/CCCA. 2011.6031525

[8] Haseeb, L., Mo, Y., & Mudasser, M. (2023). A Review The Research Status of Switched Reluctance Generator. *Diyala Journal of Engineering Sciences*, *16*(4), 1-19. https://doi.org/10.24237/djes.2023.160401

[9] Ibrahim, M. N., Nonneman, J., Mohamed, A. H., Daem, A., Abdallh, A. A., Schlimpert, S., & Sergeant, P. (2020, August 23-26). *Directly cooled windings in switched reluctance machines.* IEEE International Conference on Electrical Machines (ICEM). https://doi.org/10.1109/ICEM49940.2020.9270925

[10] Vujičić, V. P. (2011). Minimization of torque ripple and copper losses in switched reluctance drive. *IEEE Transactions on Power Electronics*, *27*(1), 388-399. https://doi.org/10.1109/TPEL.2011.2158447

[11] Kenjo, T., & Takano, Y. (2012, October 21-24). *Comparison of torque-to-copper loss ratio in switched reluctance and induction motors for EV applications.* IEEE International Conference on Electrical Machines and Systems (ICEMS), Sapporo, Japan.

[12] Jebaseeli, E. A. E., & Susitra, D. (2010, November 13-15). Performance Analysis of various configurations of switched reluctance machine for wind energy applications. IEEE *Recent Advances in Space Technology Services and Climate Change 2010 (RSTS & CC-2010)*, Chennai, India. https://doi.org/10.1109/ RSTSCC.2010.5712880

[13] Abdollahi, S. E., & Vaez-Zadeh, S. (2013). Reducing cogging torque in flux switching motors with segmented rotor. *IEEE Transactions on Magnetics*, *49*(10), 5304-5309. https://doi.org/10.1109/TMAG.2013.2260347.

[14] Nouri, N., Zamani, A. A., Barakati, S. M., (2018). *Load frequency control with considering impact of wind turbine using a Fractional PID controller*. Smart Grid Conference (SGC), 10.1109/SGC.2018.8777880.

[15] Fleury, A., Andrade, D., Oliveira, E. S. L., Fleury-Neto, G. A., Oliveira, T. F., Dias, R. J., & Silveira, A. W. F. V. (2008, November 10-13). *Study on an alternative converter performance for switched reluctance generator*. IEEE Annual Conference of IEEE Industrial Electronics, Orlando, FL, USA. https://doi.org/10.1109/ IECON.2008.4758160

[16] Sun, J., Kuang, Z., Wu, H., Wang, S., & Ning, G. (2011, August 20-23). *Implementation of a high-speed switched reluctance starter/generator system.* IEEE International Conference on Electrical Machines and Systems. Beijing, China. https://doi.org/10.1109/ICEMS.2011.6073921

[17] Scalcon, F. P., Fang, G., Volpato Filho, C. J., Gründling, H. A., Vieira, R. P., & Nahid-Mobarakeh, B. (2022). A review on switched reluctance generators in wind power applications: Fundamentals, control and future trends. *IEEE Access*, *10*, 69412-69427. https://doi.org/10.1109/ACCESS.2022.3187048

[18] Sun, L., Vansompel, H., Zhang, Z., Ibrahim, M. N., & Sergeant, P. (2021). Comparative study of switched reluctance generators with separate field current and circulating current excitations. *IEEE Transactions on Energy Conversion*, *37*(2), 1124-1133. https://doi.org/10.1109/TEC.2021.3119694

[19] Catata, E. O. H., Neto, P. J. D. S., De Paula, M. V., Silveira, J. P. C., Barros, T. A. D. S., & Ruppert Filho, E. (2021). In-loop adaptive filters to improve the power quality of switched reluctance generator in WECS. *IEEE Access*, *10*, 2941-2951. https://doi.org/10.1109/ACCESS.2021.3136203

[20] Namazi, M. M., Koofigar, H. R., & Ahn, J. W. (2020). Active stabilization of self-excited switched reluctance generator supplying constant power load in DC microgrids. *IEEE Journal of Emerging and Selected Topics in Power Electronics*, *9*(3), 2735-2744. https://doi.org/10.1109/JESTPE.2020.2994017

[21] Lu, M. Z., Jhou, P. H., & Liaw, C. M. (2020). Wind switched-reluctance generator based microgrid with integrated plug-in energy support mechanism. *IEEE Transactions on Power Electronics*, *36*(5), 5496-5511. https://doi.org/10.1109 /TPEL.2020.3029528

[22] Kord, H., Zamani, A. A., Barakati, S. M., (2023). Active hybrid energy storage management in a wind-dominated standalone system with robust fractional-order controller optimized by Gases Brownian Motion Optimization Algorithm. *Journal of Energy Storage*, *66*(30), https://doi.org/10.1016/j.est.2023.107492.

[23] Chen, H., Xu, D., & Deng, X. (2020). Control for power converter of small-scale switched reluctance wind power generator. *IEEE Transactions on Industrial Electronics*, *68*(4), 3148-3158. https://doi.org/10.1109/TIE.2020.2978689.

[24] Zahid, A., & Bilgin, B. (2023). Determining the control objectives of a switched reluctance machine for performance improvement in generating mode. *IEEE Open Journal of Industry Applications*, *4*, 99-110. https://doi.org/10.1109/OJIA. 2023.3256364

[25] Manyonge, A. W., Ochieng, R. M., Onyango, F. N., & Shichikha, J. M. (2012). Mathematical modelling of wind turbine in a wind energy conversion system: Power coefficient analysis. *Applied Mathematical Science*, *6*(91), 4527-4536.

[26] Wasynczuk, O., Man, D. T., & Sullivan, J. P. (1981). Dynamic behavior of a class of wind turbine generators during randon wind fluctuations. *IEEE Transactions on power apparatus and systems*, (6), 2837-2845. https://doi.org/10.1109/ MPER.1981.5511593

[27] Saad, N. H., El-Sattar, A. A., & Metally, M. E. (2018). Artificial neural controller for torque ripple control and maximum power extraction for wind system driven by switched reluctance generator. *Ain Shams Engineering Journal*, *9*(4), 2255-2264. https://doi.org/10.1016/j.asej.2017.03.005

[28] Kuai, S., Zhang, H., Xia, X., & Li, K. (2019). Unipolar sinusoidal excited switched reluctance motor control based on voltage space vector. *IET Electric Power Applications*, *13*(5), 670-675. https://doi.org/10.1049/iet-epa.2018.5636

[29] Huang, C. N., & Yu, C. C. (2016). Integration of Taguchi's method and multiple-input, multiple-output ANFIS inverse model for the optimal design of a water-cooled condenser. *Applied Thermal Engineering*, *98*, 605-609. https://doi.org/ 10.1016/j.applthermaleng.2015.11.112

[30] Yi, Lz., Wang, Gp. & Wu, Jl. (2011). Research of variable speed directly driven SRG wind power system position sensorless based on DFNN by FEA. *Journal of Coal Science and Engineering (China)*, 17, 107–112. https://doi.org/10.1007 /s12404-011-0121-5.

[31] Muyeen, S. M., Al-Durra, A., Hasanien, H. M., (2015). Application of an Adaptive Neuro-Fuzzy Controller for Speed Control of Switched Reluctance Generator Driven by Variable Speed Wind Turbine. Modern Electric Power Systems (MEPS), Wroclaw, Poland, https://doi.org/10.1109/MEPS.2015.7477210.

[32] Sekhar, D. C., Rama Rao, P. V. V., Kiranmayi, R., (2022). A novel efficient adaptive-neuro fuzzy inference system control based smart grid to enhance power quality. *International Journal of Electrical and Computer Engineering (IJECE)*, 12 (4), 3375-3385. http://doi.org/10.11591/ijece.v12i4.pp3375-3387.

[33] Hong, C. M., Huang, C. H., Cheng, F. S., (2017). Design of an Adaptive Intelligent Control Scheme for Switched Reluctance Generator in Wind Energy Applications. *Engineering Computations*, *34* (1), 105-122, http://doi.org/ 0.1108/EC-10-2015-0314.

[34] Soliman, M. A., Hasanien, H. M., Azazi, H. Z., El-Kholy, E. E., Mahmoud, S. A., Hybrid (2018), ANFIS-GA-Based Control Scheme for Performance Enhancement of a Variable-Speed Wind Energy Conversion System, *IET Renewable Power Generation*, *12* (7), 832-843, https://doi.org/10.1049/iet-rpg.2017.0576.